TABLE OF CONTENTS

Page No.

HAYSTACK INSTRUMENTATION

1. Antenna System 1
2. Deformable Subreflector 3
3. Radiometric Systems 3
4. Ground Instrumentation and Support 5
   - 4.1 Telescope Control and Pointing 5
   - 4.2 Data Acquisition and Processing 6
   - 4.3 Spectrometers 6
   - 4.4 Spectrometer Data Processing 7
5. Antenna Performance Characterization 9
   - 5.1 Haystack Antenna Response to Extended Sources 14
   - 5.2 Pointing Accuracy 17
6. *Umbrella* - User Interface and Scheduling System 19

Haystack 37-m Telescope:

Description of Instrumentation Systems

1. Antenna System

The main reflector is a solid aluminum surface shell, 36.6 m in diameter, composed of 96 light, stiff panel sections. The surface deviation from a best-fit paraboloid is 0.25 mm rms, allowing observations up to 115 GHz under stable thermal conditions. Environmental control within the 45.7-m rigid radome reduces the effects of the thermal environment on pointing and efficiency.

The antenna configuration is Cassegrainian, with no prime focus capability. A deformable subreflector, 2.84 m in diameter, provides focus, tilt and translation motion under computer control for feed offsets and focus. Astigmatism and other gravitational deformations of the main reflector are compensated by a combination of computer-controlled subreflector deformation and thermal control on the main reflector. Thermal deformations caused by absolute and variable temperatures are also compensated by the thermal control system. Figure 1 shows important antenna dimensions. Main reflector focal length = 14.6 m, f/d = 0.4, magnification = 10.7.

An elevation over azimuth mount, with its hydraulic pointing servo controlled from a PC, permits full-sky coverage. Slew rate is 2 degrees per second in both axes. Pointing accuracy of ~5 arcsecs in azimuth and elevation is achieved during stable thermal conditions (e.g., winter nights). Tracking precision of 2 arcsec in both azimuth and elevation over an hour period is obtained.

The antenna structure is designed for interchangeability of instrument packages at the Cassegrainian focal point. The radiometer box contains feeds and low noise receivers for three frequency bands, as described below. The low-noise receivers are cooled by closed-cycle cryogenic refrigerators, operating at either 4 or 20 K, depending upon the system.

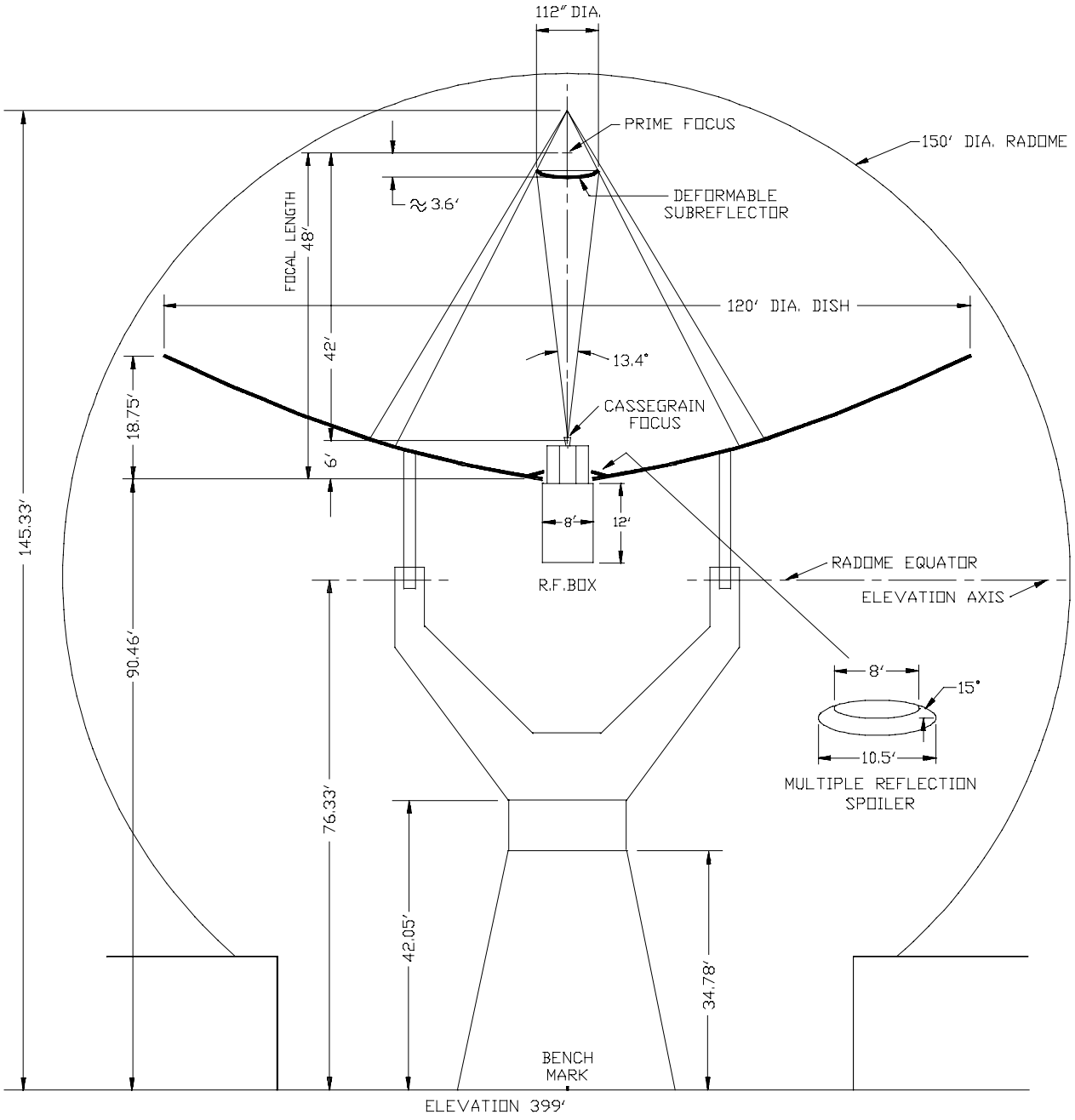

HAYSTACK CRITICAL DIMENSIONS

0' 10'
SCALE

PBS/RJC 1DEC.'72
CAD FILE: C5555ENG
LAST REV. 1JAN.'94

Figure 1

2. Deformable Subreflector

The Haystack subreflector has five positional degrees of freedom–three translations and two rotations or tilts–plus astigmatism and two rings that can be adjusted in shape. Determining whether all these parameters are optimally adjusted is a formidable task. Axial focus, astigmatism, and certain ring deformations are varied as a function of elevation and other variables to maximize antenna gain. Seven of the subreflector parameters (all except some of the ring deformations) can be "peaked" semi-automatically using the FOCUS program. Haystack staff perform this optimization operation. While pointing toward a small-diameter radio source, radiometric measurements are made by FOCUS at three values of a subreflector offset parameter, a gaussian is fitted through the three radiometric temperatures, and the fitted numbers are printed and logged.

For axial focus, vertical translation, and astigmatism–subreflector parameters prescribed to vary with elevation–the equations each have three constants, which can be considered as a zero offset, a sine term, and a cosine term. Thus a "peak" measurement at each of three disparate elevations gives, in principle, enough information to check or determine the values of the three constants. Each of the other two subreflector-position parameters, which, we assume, should not vary with elevation, is characterized by a single constant, which can be checked or determined by a single "peak" measurement. We make, in practice, many such measurements, fit parameters in a least-squares sense to the FOCUS data, and use the results as corrections to the SG&H-derived constants. "Tuning" the other subreflector-shape parameters (and the splice-plate thermal-control parameters) is done using holography at three or more elevations. The corrected parameters are then used for subsequent observing. As a result of this "tuning," the gain curve (gain versus elevation) is significantly flatter. During observations, the subreflector tuning is performed automatically, and the user is not expected to perform any adjustments.

3. Radiometric Systems

Radio astronomy receivers are housed in a radiometry box that is placed on the antenna at the Cassegrain focus. These box contains the feeds, the radiometer front ends, phase-locked local-oscillator systems, and the wide-band IF amplifiers to connect with ground-level support equipment. Systems available in the radiometry box are summarized in Table 1. Haystack is also capable of radar operations at 10 GHz, and a change between the radiometry and radar boxes on the antenna normally is accomplished with check-out in less than four hours.

Table 1

Haystack Observatory Radiometry Systems

Wavelength	**1.3 cm**	**7 mm**	**3 mm**
Frequency (GHz)	20–25	36–49	82–116
Bandwidth (MHz)**	1,000	1,000	600
Amplifier Type	Cooled HEMT	Cooled HEMT	SIS Mixers
System Temperature	120 K* (Referenced to above the atmosphere)	120–200 K* (Referenced to above the atmosphere)	200–400 K SSB* (Referenced to above the atmosphere)
Polarization	Circular	Linear or Dual linear at 36.5–43 GHz	Dual Linear Dual Circular
Switching System	Frequency	Frequency, Offset Beam	Frequency, Offset Beam
Remarks	Spectroscopy or Continuum	Spectroscopy or Continuum	Spectroscopy, Continuum or VLBI

Note: All spectral line systems can operate unswitched with observations on- and off-source.
*Depending on frequency and for clear, dry weather, at zenith
**Observations with B.W. >320 MHz require special set-ups

The radiometers presently available for observations, as listed in Table 1, are:

3.1. *λ1.3 cm – 20 to 25 GHz Cooled HEMT*

This cooled 22 GHz HEMT amplifier receiver is installed off-axis from the center of the radiometry box where the λ3-mm receiver is located. It has a single channel and receives circular polarization. It supports total power and frequency switched observations. System temperature is ~120 K referenced to above the atmosphere.

3.2. *λ7 mm – 36 to 49 GHz Cooled HEMT*

This dual-channel system consists of two HEMT amplifiers, one usable in the frequency band 36–43 GHz and the other usable in the band 36.5–49 GHz, allowing dual channel coverage in the 36.5–43 GHz range. System temperatures are 120–200 K depending on frequency, referenced to above the atmosphere. Linear polarization is received; frequency and beam switching are possible.

3.3. *λ3 mm – 82 to 116 GHz*

The dual-channel radiometer used for λ3-mm observations simultaneously receives two linear or two circular polarizations by using two tunable SIS mixers followed by HEMT IF preamplifiers. These components, and the feed horn assembly, are all cooled to 4 K by a closed cycle refrigerator. The mixers can be tuned for single sideband performance in the 82 to 116 GHz range with bandwidths of several hundred MHz. Noise temperatures, referenced to above the atmosphere, vary with frequency from about 200 K at the low end of the frequency band to about 400 K at the high end, where the atmosphere is a significant loss. Local oscillator power for the mixers is generated by a phase-locked oscillator suitable for spectral line and VLBI observations.

Continuum, spectral line, and VLBI observations are all possible. Observing modes include total power, frequency switching, and beam switching. While beam switching, a motor driven reflector disk is used to switch between two beams separated by 7 arcminutes at rates of 5–20 Hz.

4. Ground Instrumentation and Support

4.1 *Telescope Control and Pointing*

A PC running Linux OS controls the Haystack antenna pointing. Pointing inputs can be in azimuth and elevation or right ascension and declination for any epoch. Ephemerides for the sun,

moon and planets are available, and special ephemerides (e.g., for comets) can be generated. Pointing offsets due to all known and reproducible effects are corrected based on surface meteorological measurements. A variety of scans and offsets can be superimposed on the pointing. Area scans of several types are available for mapping, and a discrete-source scan (DSS) routine or a five-point routine can be used for determining source positions and amplitudes.

Haystack's primary time and frequency standard is a hydrogen maser that is capable of supporting VLBI experiments; all our local oscillators are phase-locked to this maser. Velocity steering of the local oscillators for spectroscopy can be computer controlled and updated every few seconds.

4.2. *Data Acquisition and Processing*

Data-acquisition through the HPC is controlled by the *Umbrella* system according to directions from users, as described in Section 6. Data-processing programs in the computer *fourier* and other computers are available to investigators. Continuum-processing programs allow examination of pointing, generation of pointing-correction parameters, flux measurements, and data editing.

Interfaces between the computer *yoda* and various hardware devices allow monitoring of cryogenic systems and thermal gradients on the telescope. Meteorological data are routinely monitored and used for calculation of and correction for atmospheric refraction and extinction. Numerous instruction and documentation files for users are available on the Web.

4.3. *Spectrometers*

A 4096-lag autocorrelation spectrometer is available. The spectrometer has four independent 1024-lag modules, which process 3-by-3-level data at up to 40 M samples/s, and has four video converters usable in many different modes. The HPC services the correlator in response to commands and header information from *Umbrella*. The HPC controls the correlator and retrieves autocorrelation numbers from it, performs Fourier transforms and other tasks for data acquisition, and provides a quick-look display of spectra on X terminals or X-rated machines locally or over Internet. Users can access and view spectra in almost real time from anywhere over Internet.

The capabilities of the Haystack autocorrelation spectrometer, which comprises four 160-MHz video converters and four modules, each with up to 1024 lags configurable in several ways, are shown in Table 2. Standard bandwidths are 160 MHz and exact ⅓ multiples down to 0.66 MHz. Two video converters can be connected to two receivers (two polarizations) to give two simultaneous spectra that, for unpolarized sources, can be averaged together to approximately double the effective integration time. Or two video converters can be offset in frequency with some overlap to place them end-to-end

in frequency (the so-called hybrid mode) to give a total effective bandwidth of up to about 290 MHz.

4.4. *Spectrometer Data Processing*

Haystack spectra can be exported to at least two data-reduction packages: CLASS (from the Grenoble group) and DRAWSPEC (from Harvey Liszt at NRAO). CLASS runs on Linux machines, on Sun 4s and on VAXes and can read certain FITS files. CLASS can read and average spectra, unfold frequency switching, fit gaussians and baselines, make screen and paper plots, and perform most of the other usual data-reduction tasks. We have a series of programs that produce CLASSy FITS files from Haystack spectra. The program Fits5 runs on fourier, reads Haystack-format spectra, and writes CLASSy FITS. DRAWSPEC, written in Turbo Pascal by Harvey Liszt of NRAO, runs on IBM PCs or compatibles under DOS or Windows, reads spectra in its own format, and performs all the essential data-reduction tasks such as averaging spectra, fitting baselines and gaussians, making screen and paper plots, and so on, as described in the manual "The DRAWSPEC system is a production of the NRAO' single dish initiative" by H.S. Liszt, 1988. The program DrawS runs on fourier or Suns, reads Haystack-format spectra, and, with certain limitations, writes spectra in DRAWSPEC format. See the memo "DRAWSPEC Support," revised 1992 July 24. Several shell scripts are available to facilitate translating Haystack spectra into these other formats.

Most investigators want to transfer spectra to their own computers and process there. Spectra in any of these formats can be written to IBM-PC-compatible (MS-DOS-compatible) or Linux-compatible floppy disks, DDS DAT tapes, zip disks or CD-Rom disks in several formats and, of course, transferred over Internet using, for example, ftp. We archive all spectra in Haystack format using tar to DAT tape, and we plan to keep these archive tapes indefinitely. All the programs cited above are in the public domain, and copies are available for investigators to install on their own machines.

Table 2. Haystack's Spectrometer's Capabilities

Label MHz	(Full) Bandwidth MHz	(8192) Point Spacing kHz	One Video Converter Lags	One Video Converter (Uniform) Resolution kHz	Two Video Converters Lags (each)	Two Video Converters (Uniform) Resolution kHz
160	160.0000	19.53125	512	377.1	256	754.2
53.3	53.3333	6.51042	1024	62.85	512	125.70
17.8	17.7778	2.17014	4096	5.237	2048	10.475
5.9	5.9259	0.72338	4096	1.746	2048	3.492
1.98	1.9753	0.24113	4096	0.5819	2048	1.1639
0.66	0.6584	0.08038	4096	0.1940	2048	0.3880

5. Antenna Performance Characterization

We measure gain or aperture efficiency of the Haystack antenna using planets such as Venus, Mars, Jupiter, or Saturn. Their brightness temperatures, angular sizes, and angular positions are well known. At λ6 mm and longer wavelengths, the beamwidth is typically larger than the planets, and the corrections for beam broadening are small. At λ3 mm, Jupiter is so large that we cannot trust the angular-size correction for aperture efficiency, but it yields information about beam efficiency.

The peak aperture efficiency measured in this way under stable thermal conditions in winter can be compared with values obtained at other wavelengths and with calculations as shown in Figure 2. The solid lines are from earlier Ruze-formula estimates, and the dashed lines are from our program APEFF, which incorporates our best estimates for all the antenna and radome parameters at the present time. At λ13 mm and longer wavelengths, noise-tube calibration is available and we correct for atmospheric attenuation using the Resch model atmosphere based on surface meteorological measurements; at shorter wavelengths, we use vane calibration. The two versions of the dashed line correspond to calibrating with a noise tube or a vane. The vane-calibration scheme converts that part of the ambient-temperature losses that are outside the vane (e.g., atmosphere and radome) from aperture efficiency to system temperature. Vane calibrations thus give higher aperture efficiencies and higher system temperatures (by the same factor) compared with noise-tube calibrations.

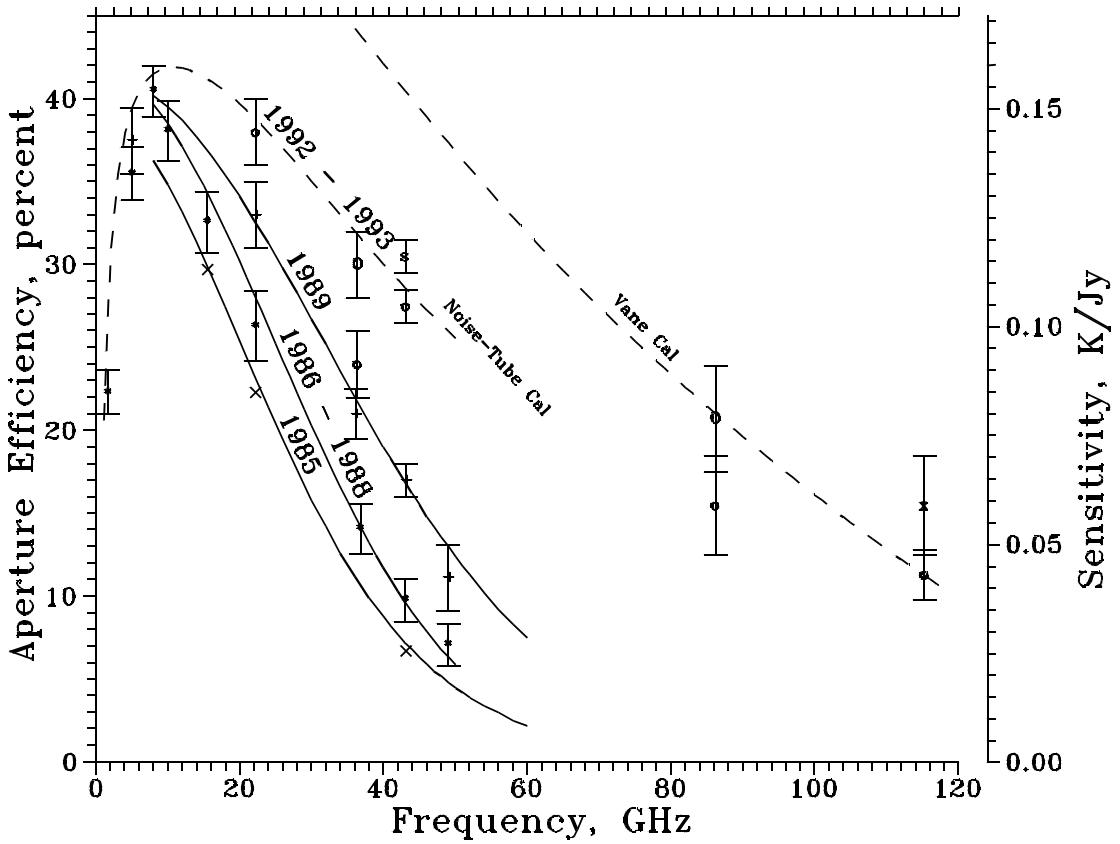

Figure 2

Using the vane-calibration scheme mentioned above, we observed Mars when it was small in angle compared to the beamwidth and inferred a peak aperture efficiency at 115 GHz (λ2.6 mm) of 11.3±1.5%. From measurements on Venus and Jupiter, which were comparable or large compared to the beamwidth, we inferred a peak beam efficiency of 16.9±2% and a peak aperture efficiency of 15.5±3% at 115 GHz, as shown by the "x" in Figure 2. At 86 GHz (λ3.48 mm), similar measurements gave a peak beam efficiency of 18±3% and a peak aperture efficiency of 16±3%. This is lower than otherwise expected because our λ3-mm feed is optimized for about 112 GHz and is well away from optimum at 86 GHz. The situation at 36.4 GHz is comparable: Our λ7-mm feed is optimized for 43 GHz. The small circles at these two frequencies show our measurements and the large circles, which should lie on the dashed curve, represent our best estimate at what an optimum feed would give. At 43 GHz, we plot Saturn values separately with an "s" because we suspect that its rings are appreciable and not properly taken into account.

Figure 3 shows a beam map made with the Haystack telescope on 1992 December 22.

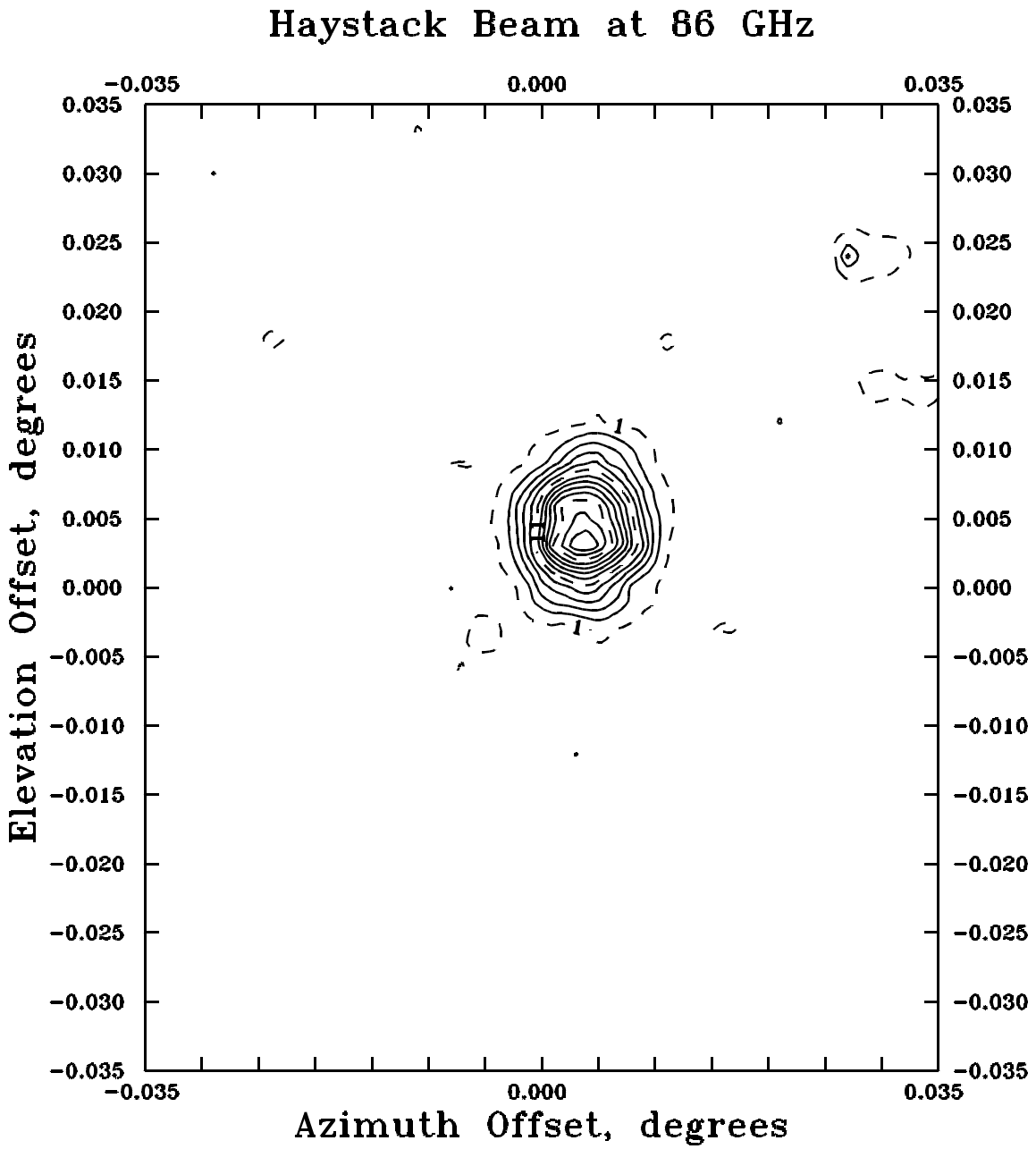

Figure 3

The target was the 15.3-km/s feature of the SiO maser at 86.2 GHz (λ3.48 mm) toward Orion IRC2. The elevation range was 33° to 36°. The amplitude scale is arbitrary but proportional to power. The peak in these units is 23.4 and the lowest plotted contour is 1. The dashed contours are at 1, 11, and 21. The apparent beamwidth (full width to half power) in this map is about 0°.0086 (elevation) or 0°.0072 (azimuth), and the calculated beamwidth (1.2λ/*D*) is 0°.0065. The azimuth axis in Figure 3 is labeled in coordinate offsets but scaled for cosine of elevation so that contours should be approximately round. Out-of-round contours can result either from actual beam shape or from pointing errors over the duration of the map–about a half hour.

Figure 4 shows some measurements toward the 86-GHz SiO maser in R Leo, which is small in angle compared to our beam. We interpreted these data as relative gain and fitted them with two versions of a gain curve. Our traditional equation is:

$$G = \exp\left[\{-S(E-E_0)^2 + U(E-E_0)^3\}F^2\right]$$

where G is the relative gain normalized to unity when the elevation, E, equals E_0, a constant. F is the observing frequency, and S and U are empirical constants related to the additional departure of the surface from a paraboloid as E moves away from E_0. This form was chosen so that S and U are normally positive. When U is zero, this equation is a Gaussian centered on E_0; a non-zero U skews the Gaussian to one side. A least-squares fit for U = 0 yielded T_0 = 51.4°K, E_0 = 40°.3, and S = 8.713E-8 for F in GHz. This equation with these constants is plotted in Figure 4 as a solid curve.

Another version of the gain equation, this one with more physical significance, is:

$$G = \exp\left[-(4\pi/\lambda)^2\{s^2(\sin E - \sin E_0)^2 + c^2(\cos E - \cos E_0)^2\}\right]$$

The wavelength, λ, is in the same units as s and c, which characterize the additional departure of the surface from a paraboloid as E moves away from E_0. This equation fits best with T_0 = 52°K, E_0 = 39°, s = 18 mils, and c = 11 mils. This equation with these constants is plotted in Figure 4 as open boxes (□). Comparison with data taken prior to installing the new subreflector shows that the gain curve is now notably flatter, and S is smaller by a factor of 3 to 5.

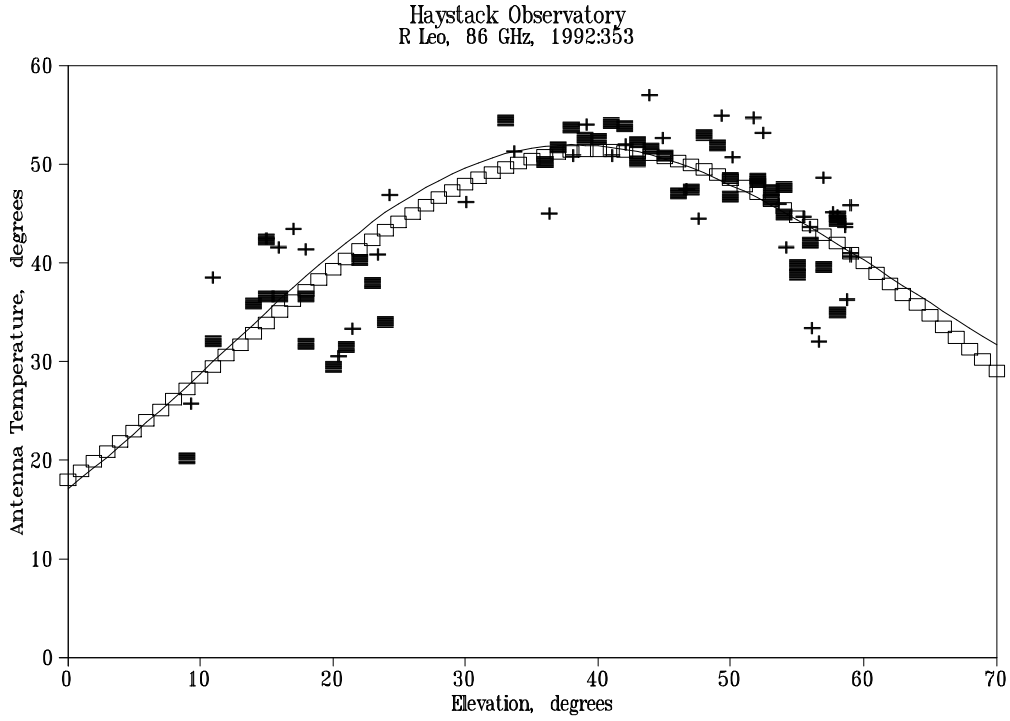

Figure 4

For sources that are not small with respect to the main beam, the gain curve *S* value may be smaller than that quoted for R Leo. Investigators may wish to derive their own gain curve during their observations. Further information and advice may be obtained from the Observatory staff.

Figure 5 shows the peak beam dilution as a function of angular size for sources at 86 GHz (λ3.48 mm). We define beam dilution as the ratio of the measured antenna temperature to the source brightness temperature. The data in Figure 5 are from Mars, Jupiter, and Venus; we avoid using Saturn because we suspect that its rings confuse the measurements at perhaps the 10% level. Data in plots such as this have error bars in both abscissa and ordinate because the beamwidth can vary and needs to be measured. Beamwidths inferred from scans through sources such as planets whose angular size is comparable to a beamwidth have very large error bars. We use, instead, beamwidths measured on small-diameter sources or calculated. The right-most datum in Figure 5 has particularly large error bars. The curve in Figure 5 is based on modeling the source as a uniform disk and the beam as a single Gaussian whose width is $1.2\lambda/D$ and whose amplitude is the aperture efficiency, 16%, indicated by the horizontal line.

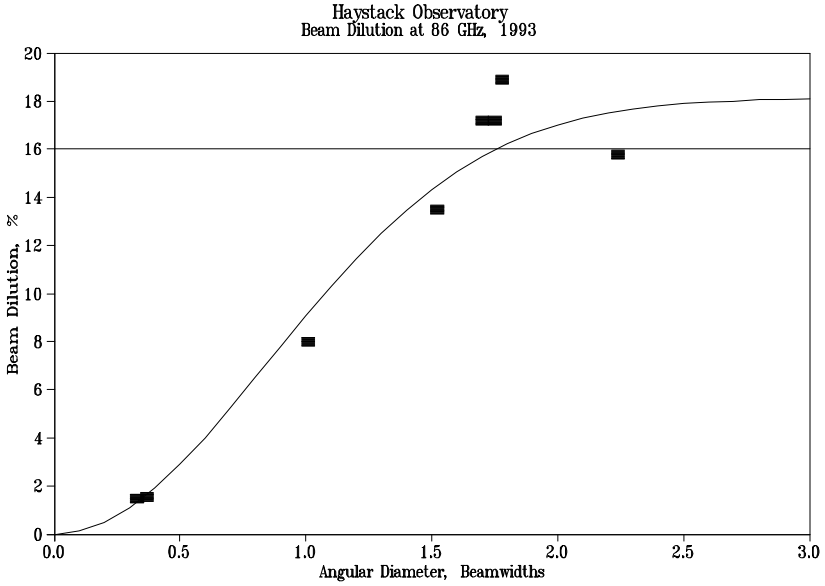

Figure 5

5.1 *Haystack Antenna Response to Extended Sources*

It is possible to characterize the antenna beam response via direct mapping of a celestial radio source, through scans across the sun or moon, and via fourier inversion of holographic maps with appropriate scaling of the phases to the frequency of interest. An example of the first method has already been given (Figure 3), but the SNR in that case is not sufficient to detect the error beam beyond a couple of beamwidths. Holography and sun scans have much higher sensitivity, and can be used to characterize the beam out to about 40 HPBW in the case of the former, and to well over 100 HPBW for the latter. An azimuthally averaged error beam at 115 GHz from holography, and a model for the error beam based on the sun scan response, is given in Figure 6.

A four-gaussian model for this measured error beam has been convolved with simple simulated sources of various widths. The sources are assumed to be circular on the sky and possessing sharp edges. Figure 7 shows four examples, with source widths from ranging 5 HPBW to 50 HPBW. The model source has a rectangular profile normalized to one, and the beam convolution, also normalized,

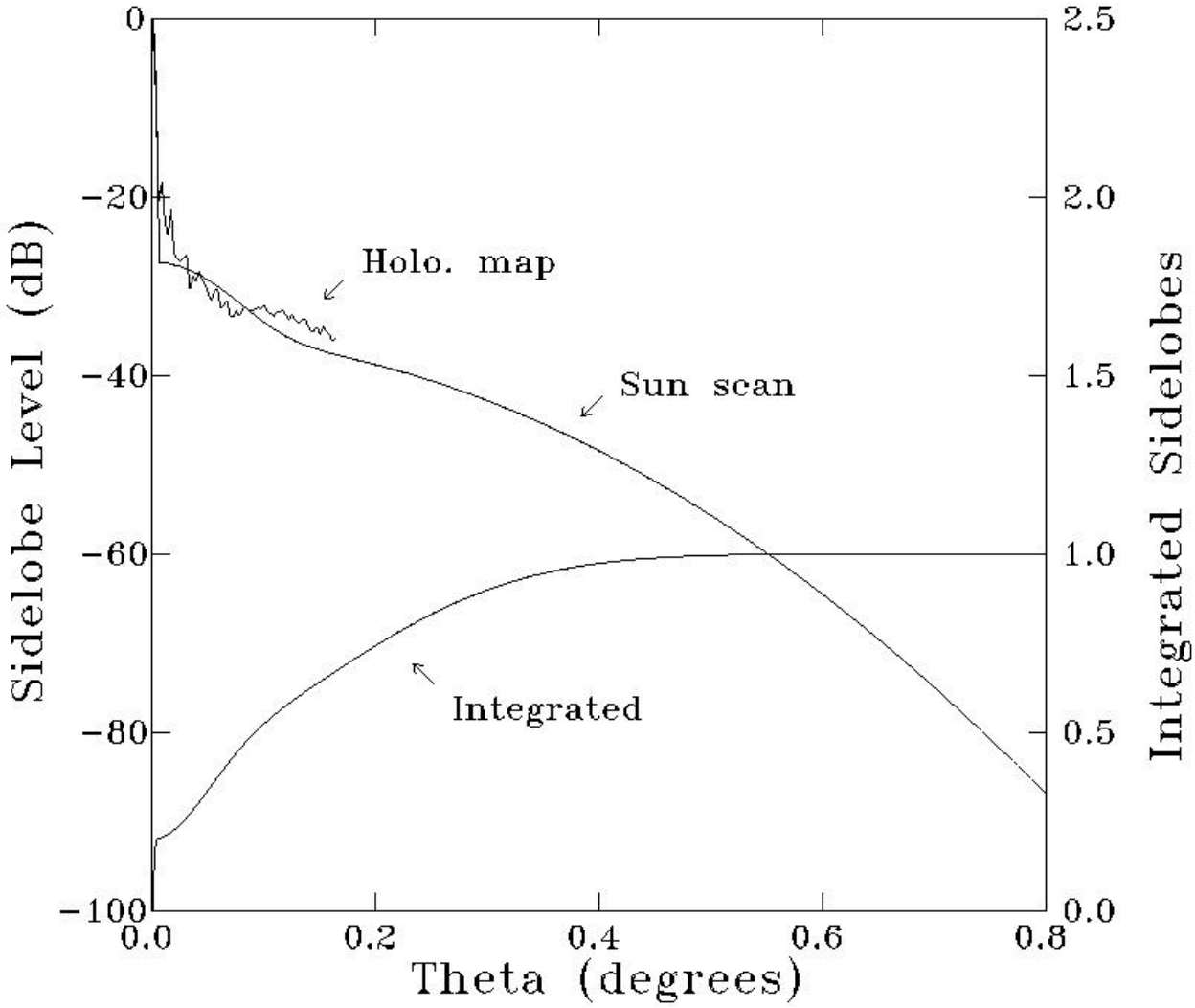
0
−20
−40
−60
−80
−100
Sidelobe Level (dB)
2.5
2.0
1.5
1.0
0.5
0.0
Integrated Sidelobes
Holo. map
Sun scan
Integrated
0.0
0.2
0.4
0.6
0.8
Theta (degrees)

Figure 6

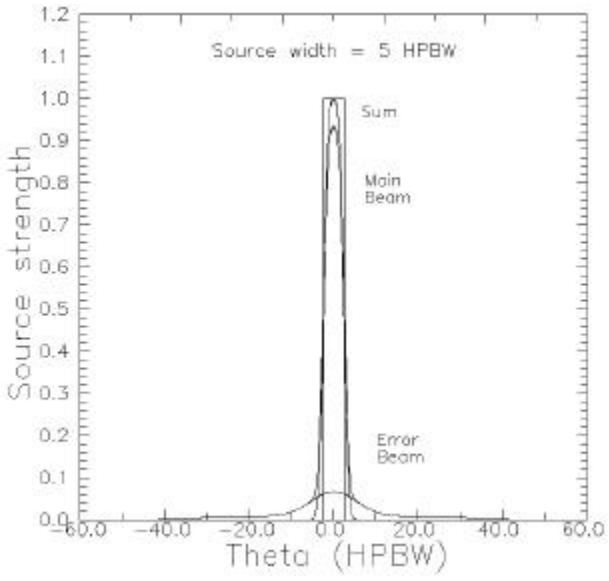
Source width = 5 HPBW
Sum
Main Beam
Error Beam
Source strength
Theta (HPBW)

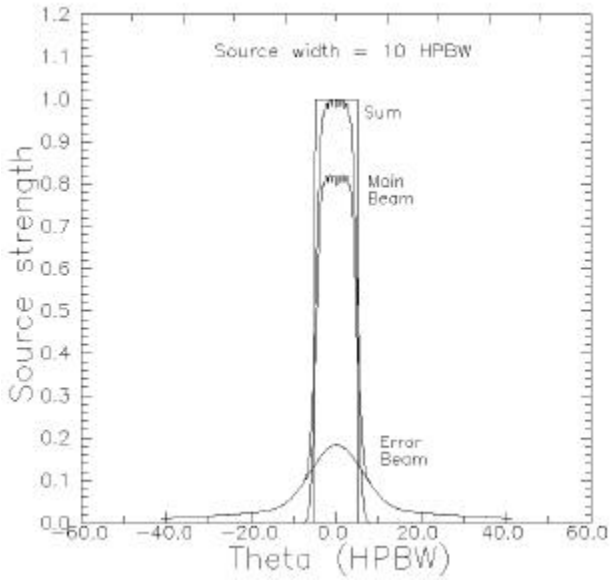
Source width = 10 HPBW
Sum
Main Beam
Error Beam
Source strength
Theta (HPBW)

Figure 7

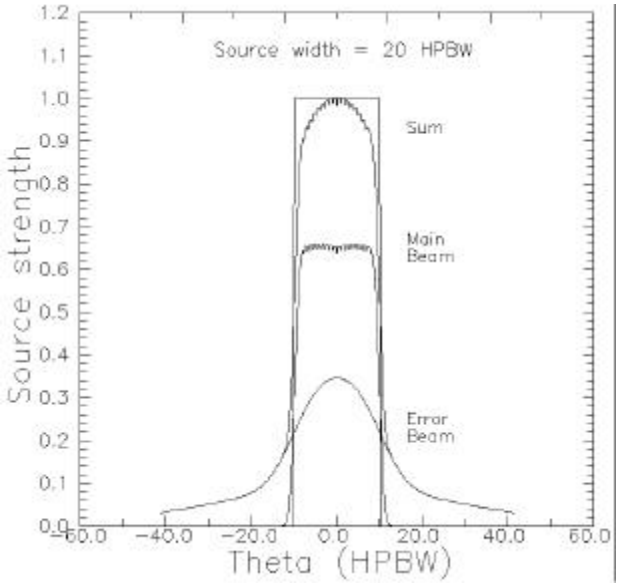
Source width = 20 HPBW
Sum
Main Beam
Error Beam
Source strength
Theta (HPBW)

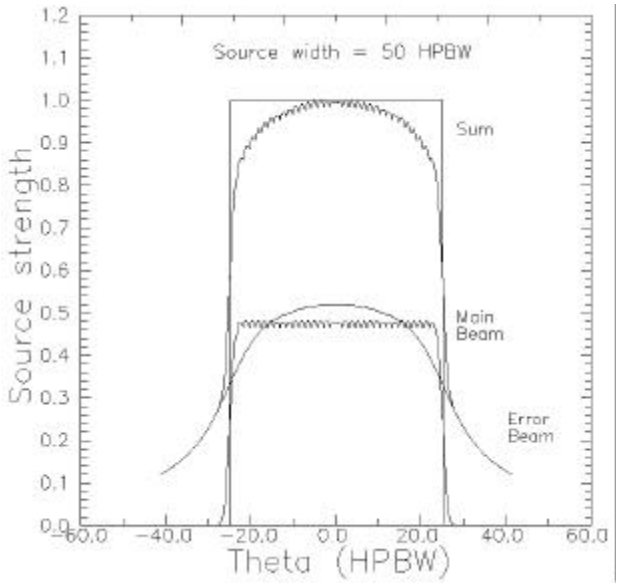
Source width = 50 HPBW
Sum
Main Beam
Error Beam
Source strength
Theta (HPBW)

is represented by three curves, the error beam contribution, the main beam contribution, and the sum of these two. At 10 HPBW, the main beam contribution dominates that of the error beam, but at 50 HPBW the two are about equal. These simulations are intended as a guide for evaluating the feasibility of individual observing projects. At frequencies below 115 GHz the ratio of main to error beam responses will be higher.

5.2 *Pointing Accuracy*

Figure 8 shows an example of the tracking performance of the antenna for an hour on a single source. Here the RMS is about 1.5 arcseconds in elevation and 1.7 arcseconds in azimuth. The beamwidth at 115 GHz is about 18 arcseconds. Summer daytime pointing is more variable due to thermal gradients across the antenna structure. Figure 9 shows an example of Haystack's pointing performance toward four sources over a ten-hour period. The RMS is about 3 arcseconds in elevation and 4 arcseconds in azimuth. This performance can be obtained when the temperature of the antenna structure is constant, good weather conditions prevail, and the pointing model has been updated recently. It is, of course, advisable to check and update the pointing using nearby pointing sources on a regular basis.

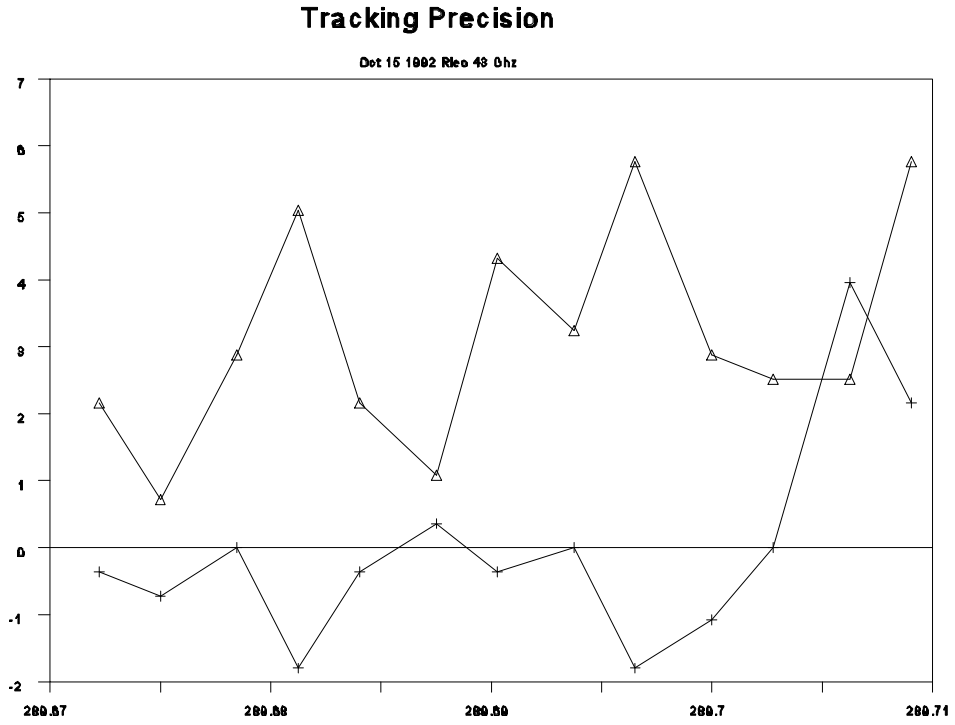

Figure 8

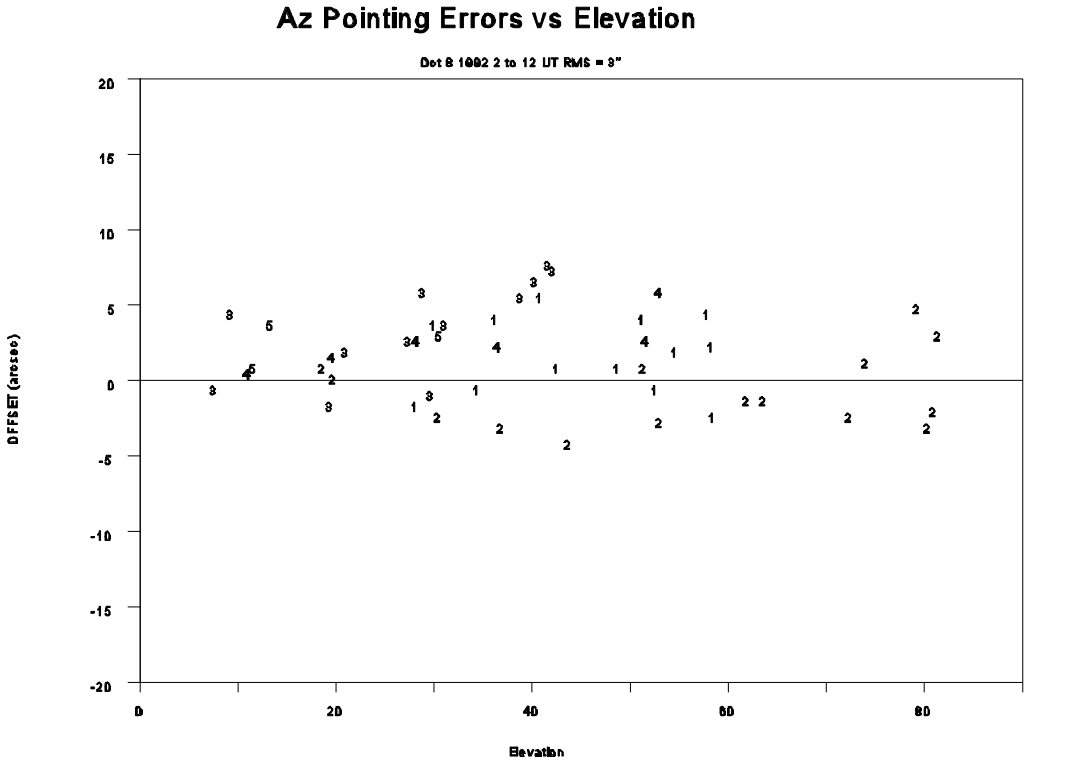
Az Pointing Errors vs Elevation
Oct 8 1992 2 to 12 UT RMS = 3"
OFFSET (arcsec)
Elevation
20
15
10
5
0
-5
-10
-15
-20
0
20
40
60
80

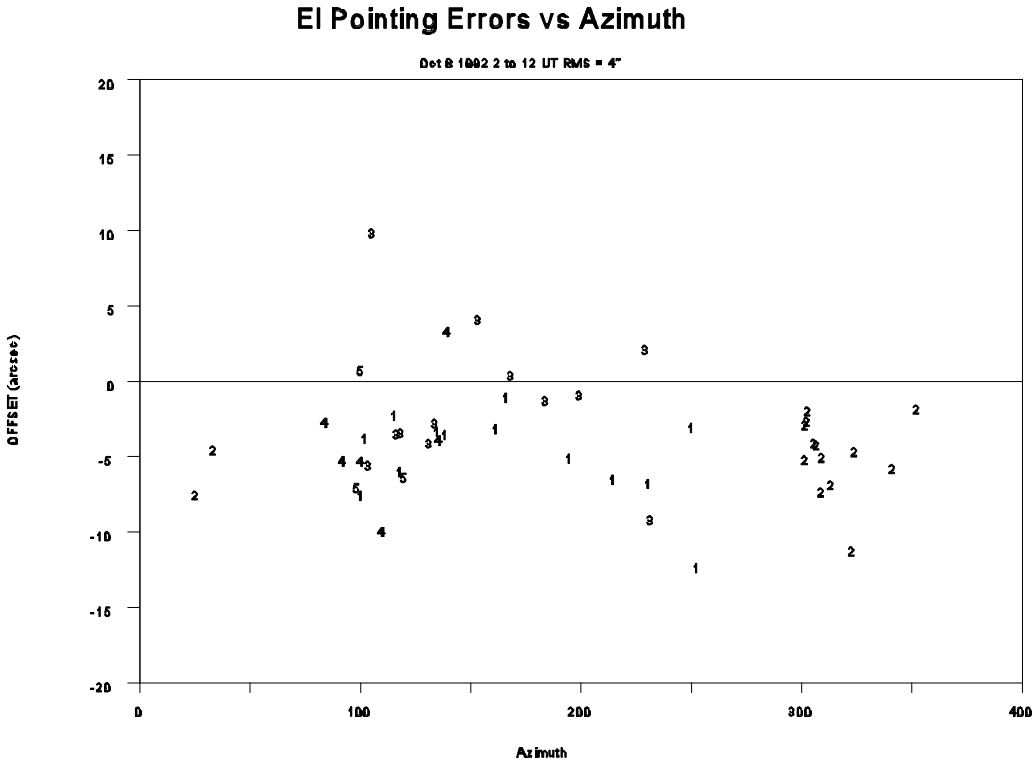
El Pointing Errors vs Azimuth
Oct 8 1992 2 to 12 UT RMS = 4"
OFFSET (arcsec)
Azimuth
20
15
10
5
0
-5
-10
-15
-20
0
100
200
300
400

Figure 9

6. *Umbrella* – User Interface and Scheduling System

Umbrella is a user interface and scheduling system for radio-astronomical observing at Haystack. *Umbrella* accepts commands typed directly or reads and executes schedule files. We have combined procedures (alias macros) and schedule into a single file and added looping and conditional constructs. The language comprises primitives and "station" macros, which are always available, and reads user-defined macros and schedules from files that can be created using any editor capable of creating straight ASCII text–no hidden codes. Such files can be typed into *fourier,* read from floppy or zip disks, or transferred over Internet.

Up-to-date and detailed information with examples on *Umbrella* is provided in the *Umbrella* manual, "*Umbrella:* A User Interaction Language for Radio Astronomy at Haystack," by J. Ball and P.J. Charpentier, a copy of the most recent version may be found here.